Fuel 161 (2015) 197–206

Contents lists available at ScienceDirect

Fuel

journal homepage: www.elsevier.com/locate/fuel

Effect of mineralogy on nuclear magnetic resonance surface relaxivity: A case study of Middle Bakken and Three Forks formations

Milad Saidian *, Manika Prasad [1]

Colorado School of Mines, 1600 Arapahoe St., Golden, CO 80401, USA

ARTICLE INFO

Article history:
Received 17 April 2015
Received in revised form 7 August 2015
Accepted 10 August 2015
Available online 24 August 2015

Keywords:
Surface relaxivity
Porosity
Pore size distribution
Nuclear magnetic resonance
Paramagnetic minerals

ABSTRACT

Porosity and pore size distribution (PSD) are crucial for reserve and producibility estimation and production planning. PSD properties are evaluated in the subsurface from nuclear magnetic resonance (NMR) logs and require knowledge about surface relaxivity. In common industry practice, a constant surface relaxivity value is used for a well, formation or rock type, regardless of mineralogical and textural variation. We present a case study of the Middle Bakken and Three Forks formations to evaluate surface relaxivity using porosity, PSD and total specific surface area data. To avoid error propagation from the input parameters to surface relaxivity estimates, we first acquired reliable porosity and PSD by combining different techniques. We analyzed the data using information on mineralogy, mass magnetic susceptibility (MMS) and scanning electron microscopy. We find that:

(a) Surface relaxivity (ρ [μm/s]) depends on paramagnetic mineral content, magnetic susceptibility and distribution in natural rocks.
(b) The linear correlation between surface relaxivity and illite content ($\rho = 0.067 \times f_{il} + 0.56$) has a goodness of fit $R^2 = 0.79$; where f_{il} is wt% of illite.
(c) This linear correlation only holds if the illite is distributed in the matrix.
(d) Clay bound water cut off times lie between 2.13–2.23 ms for T_1 and 1.34–1.40 ms for T_2 distributions based on our mineralogy-guided calculations. The commonly-used T_2 value of 3 ms results in large errors in clay bound porosity calculations (>100%) especially for high clay content samples.

Our results can help improve NMR logs interpretations for surface relaxivity, PSD and clay content evaluation in Middle Bakken and Three Forks Formations. We suggest using our methodology to find similar correlations between surface relaxivity and distributed clay content and, in turn, to calculate surface relaxivity for other formations.

1. Introduction

Logging data acquisition and interpretation play a significant role in reserve and producibility estimation and production planning. Reliable petrophysical models require accurate estimation of petrophysical properties such as porosity and pore size distribution (PSD). NMR logging is widely used to measure the porosity and PSD in the form of longitudinal (T_1) and transverse (T_2) relaxation times [46]. Surface relaxivity is used to convert NMR time distributions to PSD. This surface relaxivity is normally assumed to be constant when interpreting NMR data. Often, in formation evaluation, representative cores from each formation are used to estimate formation-specific surface relaxivity. NMR log interpretation can be improved significantly by honoring mineralogical and textural variations in surface relaxivity calibrations.

Surface relaxivity is attributed to the paramagnetic impurities on the surface of the grains that interact with hydrogen nuclei and impose an additional relaxation [30]. Numerous studies have shown that surface relaxivity increases with increasing paramagnetic content such as manganese and iron [14,22] or iron bearing minerals such as pyrite, pyrrohotite and siderite [24]. Iron bearing minerals and iron oxides have significant effect on surface relaxivity. However, the common industry practice of calculating surface relaxivity based on a limited number of samples ignores variations in rock composition. The calculated values of surface relaxivity have been found to vary significantly, up to one order of magnitude for the same rock type or porous material [19,12,13].

* Corresponding author. Tel.: +1 (303) 273 3457 (office); fax: +1 (303) 273 3189.
E-mail addresses: msaidian@mines.edu (M. Saidian), mprasad@mines.edu (M. Prasad).
[1] Tel.: +1 (303) 273 3457 (office); fax: +1 (303) 273 3189.

http://dx.doi.org/10.1016/j.fuel.2015.08.014
0016-2361/

Calculation of surface relaxivity using theoretical models requires an estimation of the electron-spin relaxation times for the paramagnetic impurity. This information is not available for the electron-spins on the surface of the rocks [28]. The methods to estimate surface relaxivity in reservoir rocks can be divided in three types; (a) Iterative variation of surface relaxivity to match NMR relaxation times with independent measurements of pore or throat size distribution, for example, from mercury intrusion capillary pressure (MICP) [36,29,27,49,39], nitrogen adsorption [39], and image analysis [18,27,21]. (b) Estimations of surface relaxivity using rock surface area measured by cation exchange capacity (CEC) [42], nitrogen gas adsorption [42,17,19], and image analysis [17]. (c) Estimation of surface relaxivity solely relying on combination of NMR measurements, namely relaxation time distribution measurements using CPMG or IR pulse sequences and restricted diffusion measurements pulse sequences such as pulse field gradient (PFG) and pulse field gradient stimulated echo (PFGSE) [38,33,19,43].

Type (c) measurements are not suitable for unconventional and tight samples because NMR data acquisition and interpretation, especially diffusion measurements, are more complicated in these rocks due to the presence of small pores and fast relaxation of hydrogens [41]. Type (a) and (b) are indirect measurements of the surface relaxivity and depend on other parameters such as pore volume (porosity), surface area and PSD. Saidian et al. [40] showed that porosity and PSD values in shales vary significantly, depending on measurement techniques. Numerous studies have focused on surface relaxivity variations in synthetic unconsolidated porous media. However, to our knowledge, a thorough study that presents surface relaxivity measurements in sedimentary rocks using different techniques and that investigates the effect of mineralogy and paramagnetic impurities on such measurements. Such an analysis to correlate the mineralogy with surface relaxivity can provide more reliable surface relaxivity values for log analysis, and consequently, more accurate PSD calculations and petrophysical interpretations.

In this study, we measured the porosity for 28 samples from Middle Bakken and Three Forks formations with various techniques, such as nitrogen adsorption (N2), NMR, water immersion (WI), and mercury intrusion (MI). Using a systematic comparison of porosity values, we investigated the reliability of PSD measured by MI, NMR and N2 techniques. We then calculated surface relaxivity by correlating the PSDs and the measured surface to volume ratios (SVR) with NMR responses. Finally, we evaluated the effect of paramagnetic impurities such as illite, chlorite and pyrite content on surface relaxivity and determined clay bound cut off values.

2. Materials

Twenty eight samples were taken from Middle Bakken and Three Forks Formations (Henceforth referred as Bakken Formation). The samples (Table 1) were carbonate rich, with mainly dolomite, and contained moderate amounts of clay and quartz or feldspar (Fig. 1). The clay type in the mixed layer illite–smectite was mainly illite.

3. Methods

We measured porosity and PSD using multiple techniques such as NMR, MI, N2, HE and WI. As received cleaned and dried core plugs were used for magnetic susceptibility and HE porosimetry. The samples were then saturated and used for NMR measurements. Finally, the core plugs were cut into aliquots. Two sets were used for WI and MI measurements. Three sets were crushed for N2, XRD and CEC measurements. In the following, we briefly explain the experimental procedure and data acquisition parameters for each technique.

Table 1
Summary of all results. TSSA: total specific surface area, TPV: total pore volume, N2 ADS DLM: logarithmic average of the PSD calculated from N2 adsorption branch, MI D_{LM}: logarithmic average of PSD calculated from MI, BMS: Bulk Magnetic Susceptibility. The grain density in this table is an average of WI and XRD calculated grain densities.

Sample #	N2 Porosity p.u.	MI Porosity p.u.	WI Porosity p.u.	NMR Porosity p.u.	Grain Density gr/cm^3	N2 BET TSSA m^2/gr	TPV cm^3/gr (10^{-3})	CEC meq/100 gr	CEC TSSA m^2/gr	T_{2LM} ms	N2 ADS D_{LM} nm	MI D_{LM} nm	BMS SI (10^{-6})	Clay Content wt%
1	2.91		3.89	5.05	2.72	2.24	10.78	2.69	20.45	2.59	30.96		88.23	5.4
2	6.53		6.91	7.97	2.72	6.80	25.25	4.27	32.44	2.59	25.36		88.64	14.4
3	1.63	2.88	3.11	2.42	2.70	1.70	6.17	0.50	3.76	7.26	25.41	90.76	12.92	1.9
4	3.10		4.38	4.12	2.68	5.69	11.79	2.55	19.37	5.06	16.19		59.95	3.6
5	1.09	1.93	2.46	2.68	2.71	1.47	4.09	0.50	3.79	4.68	20.82	36.67	27.06	2.0
6	6.69		5.13	5.05	2.68	8.52	26.43	3.96	30.11	2.93	20.70		63.74	7.9
7	5.49		4.73	5.58	2.67	6.14	21.33	1.80	13.69	2.74	22.62		74.81	9.3
8	3.34			3.82		3.21	12.63	2.23	16.95	2.59	12.20		32.92	8.6
9	5.28	6.85	7.98	6.08	2.71	4.70	20.60	2.35	17.86	2.57	13.05	42.07	64.01	11.3
10	4.93		3.97	5.09	2.69	4.75	19.00	1.81	13.76	2.79	28.83		62.23	12.2
11	6.05			5.30		5.78	23.61	3.61	27.42	2.59	21.56		64.13	9.8
12	4.31	5.30	5.29	4.72	2.68	4.73	17.02	1.67	12.66	2.58	22.61	36.54	68.45	10.3
13	4.63			5.43		4.34	17.79	3.27	24.86	2.81	12.51		62.18	11.1
14	6.07		4.94	5.58	2.71	5.70	23.54	3.28	24.92	2.63	13.48		66.80	14.8
15	6.60	7.78	6.43	8.05	2.78	5.99	25.98	2.80	21.31	2.53	14.97	26.24	96.63	19.8
16	3.79	4.21	4.67	3.64	2.79	2.90	14.36	1.66	12.61	5.41	18.77	49.85	65.11	4.0
17	3.12			6.19		2.53	11.40	2.95	22.43	3.11	14.57		93.71	10.5
18	1.09	1.85	2.67	2.75	2.81	0.81	3.94	0.67	5.06	12.43	18.64	64.87	57.29	2.5
19	1.42	3.00	3.01	3.81	2.80	0.97	5.22	1.49	11.29	5.73	25.36	58.83	66.29	5.6
20	8.08	6.10	7.68	8.12	2.79	8.56	31.76	3.26	24.80	1.78	11.18	13.40	162.94	32.1
21	7.46	4.99	7.15	7.84	2.78	7.85	29.25	2.22	16.86	2.89	17.28	26.43	166.91	20.3
22	9.09	5.71	7.90	7.13	2.81	9.49	35.90	1.84	14.01	2.07	11.44	18.45	145.68	17.7
23	7.23		5.26		2.80	5.51	27.24	2.11	16.07	0.62	16.15		189.80	20.0
24	8.97			9.08		8.53	35.06	3.29	25.03	2.18	13.67		236.46	25.7
25	6.54			8.93		5.53	24.94	2.63	19.96	1.79	14.78		216.30	17.9
26	9.40	4.86	6.90	7.71	2.78	8.36	37.59	3.04	23.13	1.77	14.33	16.23	111.06	25.0
27	8.86			8.85		8.36	34.75	2.53	19.25	1.81	13.99		259.43	28.8
28	11.07			11.15		11.94	44.50	3.29	25.03	1.89	12.32		246.65	28.5

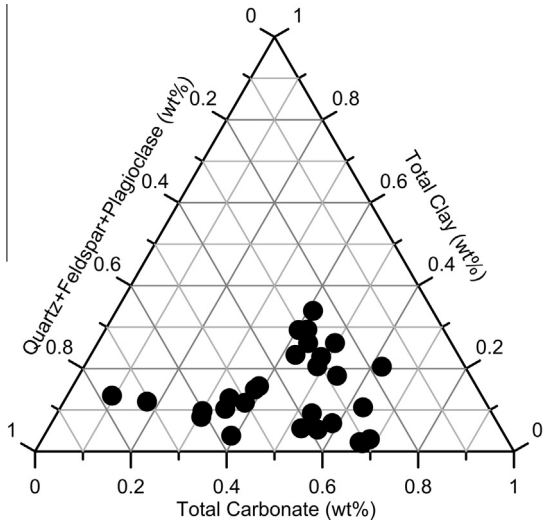

Fig. 1. Mineralogy of the Bakken samples. 28 samples were taken from Middle Bakken and Three Forks formations. Samples were carbonate rich, mainly dolomite (up to 78 wt%) with moderate amount of clay (up to 36 wt%) and quartz + feldspars (up to 46 wt%).

3.1. Nuclear magnetic resonance (NMR)

T_1 and T_2 distributions as well as porosity were measured using inversion recovery and Carr, Purcell, Meiboom and Gill (CPMG) [6,37] pulse sequences, respectively. The samples were fully brine (25,000 ppm KCl brine) saturated and the measurements were performed using a 2 MHz Magritek Rock Core Analyzer®. All T_2 distributions were measured using 100 μs echo spacing (TE), 3000 ms polarization time, 2500 number of echoes and minimum 100 signal to noise ratio (SNR). The T_1 distributions were measured using 20 logarithmically spaced wait times ranging from 0.07 to 3000 ms. T_1 and T_2 distributions were generated using inverse Laplace non-negative least square fitting [34,5] of inversion recovery and echo train data, respectively. The smoothing parameter was calculated using the methodology described by Dunn et al. [11].

Assuming very long bulk relaxation rate (compared to surface relaxation), negligible diffusion induced relaxation, and fast diffusion regime in individual pores, the NMR response can be related to pore size using the following equations [7,12]:

$$\frac{1}{T_i} = \frac{1}{T_{is}} = \rho_i \frac{S}{V} = \rho_i \frac{c}{R} \quad (1)$$

where subscript "*i*" denotes 1 or 2 for T_1 and T_2 relaxations, respectively, ρ is the surface relaxivity, S is the rock surface area, V is the pore volume, R is the pore radius and c is the constant = 1, 2 or 3 for planar, cylindrical and spherical pores, respectively.

3.2. Mercury intrusion (MI)

Porosity and pore throat size distribution (TSD) were measured using MI technique. Small rock chips were heated up to 200 °C and degassed to remove all the water. Mercury was injected into the samples with uniform pressure steps ranging from 0.14 to 420 MPa (14.7 to 60,000 psi). The pressure data were converted to TSD using the Washburn [47] model of a bundle of non-connected capillary tubes. The Bailey method [8] was applied to the high pressure measurements for conformance correction for mineral compressibility.

3.3. Nitrogen adsorption (N2)

Nitrogen adsorption technique was used as specified by Kuila [31] to measure total specific surface area (henceforth referred as surface area), total pore volume (henceforth referred as pore volume) and PSD for all samples. Briefly, the samples were crushed and sieved (40 mesh, equivalent to 420 μm) and degassed under vacuum at 200 °C until the out-gassing rate was less than 0.005 Torr/min over a 15 min interval. Nitrogen was injected into the degassed sample and the pressure–volume data were recorded at constant temperature (Langmuir isotherms). The Barrett, Joyner and Halenda (BJH) inversion [3] was used to calculate the PSD assuming non-connected cylindrical pores. The PSD spectra calculated using BJH span from 1.7 nm to 200 nm. Due to technical limitations N2 technique does not assess pores larger than 200 nm in width [15]. The Harkins and Jura [16] thickness curve was utilized for both BJH inversion and micropore (pores smaller than 1.7 nm) volume calculation with *t*-plot analysis.

3.4. Water immersion (WI)

Porosity was measured using water immersion technique. The Archimedes's principle was used to measure the bulk and grain volumes. The original protocol for this measurement was developed at the American Petroleum Institute (API RP40). In this study, we used the adapted protocol for mudrocks developed by Kuila et al. [32]. Five grams of rock chips were first dried and weighed in air. This weight was measured using a Mettler Toldeo® moisture analyzer at 200 °C for 15 min to exclude the weight of possible adsorbed moisture. Then the samples were saturated and weighed again in air and submerged in water.

3.5. Cation exchange capacity (CEC)

Based on the laboratory procedure provided by the vendor, CEC was measured using the Co(III)-hexamine^{3+} cation exchange, spectrophotometric technique. CEC values were converted to "smectite equivalent" by assuming a theoretical CEC of 95–100 meq/100 g of the smectitic surfaces of illite–smectite and common pure smectites. The CEC surface area was calculated from the "smectite equivalent" values assuming a theoretical surface area of 800 m^2/g of pure smectite.

3.6. Bulk magnetic susceptibility (BMS)

The bulk magnetic susceptibilities (henceforth referred as susceptibility) were measured for all samples using a Kappabridge (KLY-4S™) magnetic susceptometer applying a 200 A/m magnetic field. The samples were cylindrical core plugs and were cleaned and dried prior to the measurement. The susceptibility was measured at laboratory conditions.

4. Results

To calculate surface relaxivity (Eq. (1)), reliable values of porosity (pore volume), surface area and PSD are needed. We performed a detailed analysis of porosity and PSD measurements for all 28 samples with variable clay content ranging from 2 to more than 32 wt%.

4.1. Porosity measurement

A comparison of the porosity values measured with WI, NMR, N2, and MI (only for 12 samples) techniques (Table 1) showed that the value lay within 2 p.u. difference. The strong positive linear correlation between the clay content and porosity (not shown here) can be used for clay content calculations using porosity measurement both at laboratory and downhole conditions. We also used a mineralogy-based model to calculate the cut off times of

2.13–2.23 ms and 1.34–1.40 ms for T_1 and T_2 distributions, respectively. These values are much lower than the common 3 ms T_2 cut off time that is used for clay bound water volume calculations [44].

4.2. PSD and surface area measurement

Fig. 2 shows the PSD measured by nitrogen adsorption technique color coded with clay content. Low clay samples show pore size lower amplitude and more uniform pore size distribution, whereas high clay samples show higher amplitude with a bi-modal distribution at 2–5 nm and 10–50 nm range. Kuila [31] showed that the 3 nm peak is directly correlated with the clay tactoid pores in mudrocks. The peaks at this pore size range are attributed to the clay minerals (mainly illite and chlorite). The clay content effects total specific surface area distribution as shown in Fig. 3. For clay-rich samples, the surface area distribution shows higher amplitudes in <5 nm range.

The MI TSD was also measured for 12 samples (Fig. 4). The throat size decreases with increasing the clay content. Figs. 5 and 6 show the NMR T_2 and T_1 distributions measured for Bakken samples, respectively. T_1 and T_2 distribution peaks shift to faster relaxation times with increasing the clay content. Clay-rich samples show uni-modal T_2 and T_1 distributions at 1–3 ms, while the low clay samples demonstrate bimodal distribution. The broader PSD spectra in low-clay samples indicate the presence of a wider range of pore sizes and also larger pores in these samples. We used logarithmic mean for each spectrum (Eq. (2)), to represent the T_1 or T_2 distribution.

$$T_{nLM} = \exp\left(\frac{\sum \ln(T_{ni}) \times \phi_i}{\sum \phi_i}\right) \quad (2)$$

where n is 1 and 2 for T_1 and T_2 relaxation times, respectively, T_{nLM} is the logarithmic mean of time distribution. If the T_n distribution spectrum is plotted using i number of points (bins), the ith bin has a T_n time (T_{ni}) and an amplitude which is the porosity associated with that bin (ϕ_i). T_{1LM}^{-1} and T_{2LM}^{-1} are correlated using $T_{1LM}^{-1} = 1.70\ T_{2LM}^{-1} + 0.03$ with high correlation coefficient ($R^2 = 0.80$) (Table 1).

5. Discussion

As mentioned earlier, in common industry practice, the surface relaxivity is assumed to be constant for any given formation or well. Significant inconsistencies have been reported in measured or calculated surface relaxivities for similar rock type or formation [12]. In this section we improve our understanding of surface relaxivity in the middle-Bakken Formation and the parameters that affect its by (a) Calculating the surface relaxivity using different techniques, (b) Studying the effect of rock composition and paramagnetic minerals on surface relaxivity, (c) Investigating the inconsistencies in surface relaxivity values and making recommendation for appropriate applications.

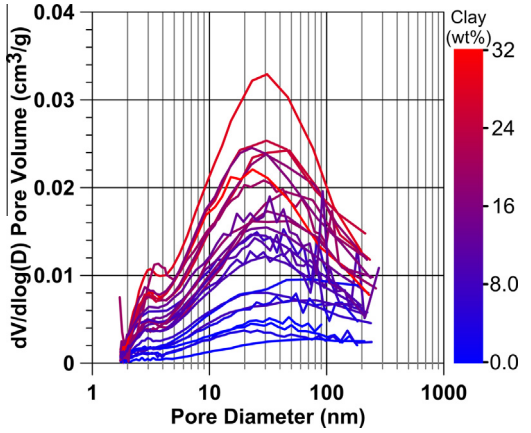

Fig. 2. Pore size distribution measured by nitrogen adsorption color coded by clay content. Clay-rich samples show higher amplitude due to higher porosity. The higher amplitude for pores in less than 10 nm range belongs to clay tactoid porosity [31]. (For interpretation of the references to colour in this figure legend, the reader is referred to the web version of this article.)

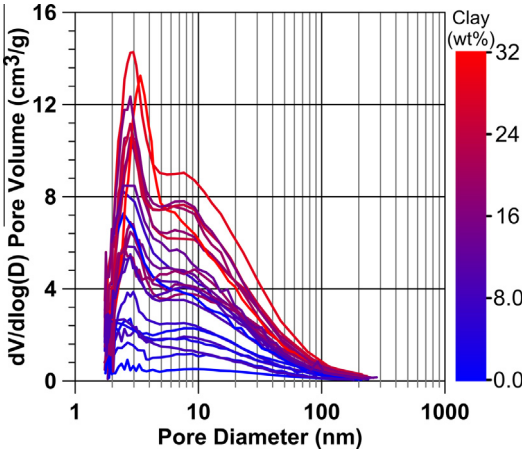

Fig. 3. Surface area distribution measured by nitrogen color coded by clay content. Clay-rich samples have higher surface area especially at smaller pores (<10 nm). (For interpretation of the references to colour in this figure legend, the reader is referred to the web version of this article.)

5.1. Surface relaxivity calculation

There are different approaches to calculate the surface relaxivity. We calculate surface relaxivity using two approaches: correlating NMR response with PSD or TSD measured by other techniques and using NMR data and Surface to volume ratio (SVR) measured independently to calculate surface relaxivity using Eq. (1). To avoid inconsistencies in the surface relaxivity calculations due to variations in porosity values measured with different techniques, we only used the surface area and pore volume measured by N2 technique for surface relaxivity calculation to study the effect of mineralogy on surface relaxivity.

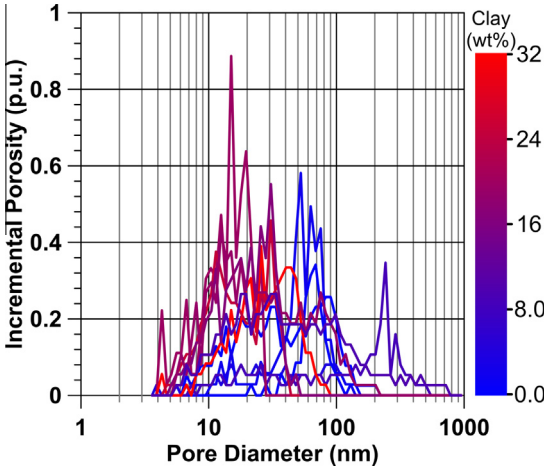

Fig. 4. The throat size distribution measured by mercury intrusion color-coded by clay content. Higher clay samples show smaller throat size range. (For interpretation of the references to colour in this figure legend, the reader is referred to the web version of this article.)

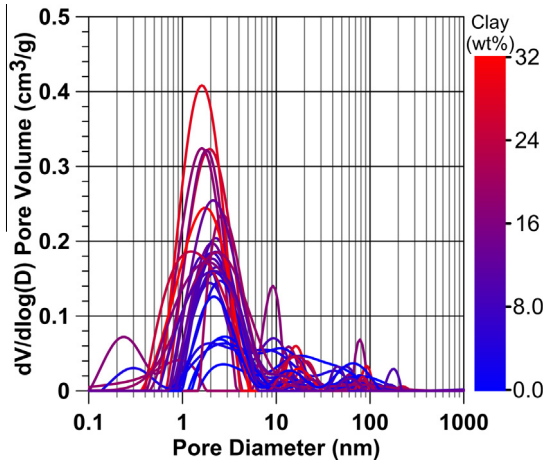

Fig. 5. Transverse relaxation time (T_2) color-coded by clay content. Low-clay samples show bimodal spectra with dominant peaks at 1–3 ms and 10–20 ms, whereas the clay-rich samples show a unimodal distribution at 1–3 ms. The logarithmic mean of the T_2 distribution decreases by increasing clay content. (For interpretation of the references to colour in this figure legend, the reader is referred to the web version of this article.)

We find that the SVR for low-clay samples (less than about 10 wt%) samples (Fig. 7) varies between 170 and 500 μm^{-1}, whereas, for the high clay content samples (Fig. 7) the SVR range is narrower – between 200 and 275 μm^{-1}. The SVR for low-clay samples depends on the pore size, whereas, SVR in clay-rich samples is dominated by clay particles (mainly illite). Clays are distributed in pores and mask the effect of pore size on the surface area measurement. Both T_1 and T_2 surface relaxivities (ρ_1N2 SVR and ρ_2N2 SVR, respectively), calculated using Eq. (1) are listed in Table 2. Note that the correlation between T_1 and T_2 can be used to convert the values from T_1 to T_2 surface relaxivity since the SVR is constant in both calculations. Henceforth we only discuss the T_2 surface relaxivity, same correlations and conclusions are applicable to T_1 surface relaxivity.

We also calculated the surface relaxivity by combination of NMR time average (T_{2LM}) and average diameter of the pores measured by MI and N2 (ρ_2 MI D_{LM} and ρ_2 N2 D_{LM}, respectively) using Eq. (1) and visual correlation of NMR time distributions with N2

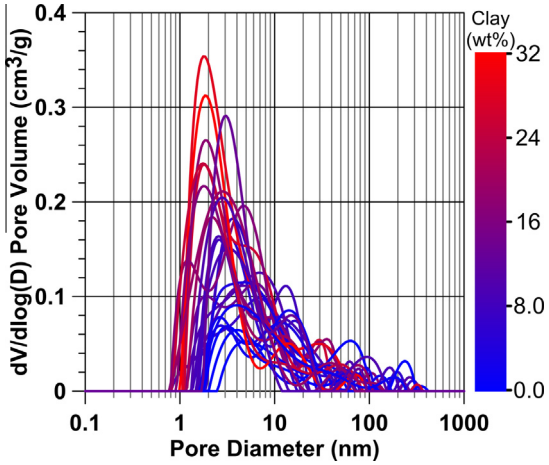

Fig. 6. Longitudinal relaxation time (T_1) color-coded with clay content. The T_1 distribution of low-clay samples shows bimodal spectra with dominant peaks at 2–4 ms and 10–30 ms, whereas the distributions for clay-rich show a unimodal distribution at 2–4 ms. (For interpretation of the references to colour in this figure legend, the reader is referred to the web version of this article.)

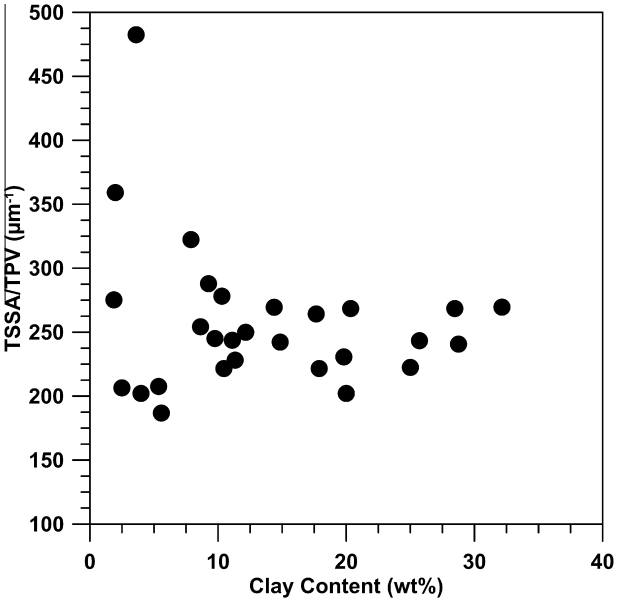

Fig. 7. Surface to volume ratio (SVR) measured by N2 technique. The SVR for low-clay samples (less than about 10 wt%) samples varies between 170 and 500 μm^{-1}, whereas, for the high clay content samples the SVR is more consistent and in the range of 200–275 μm^{-1}. The SVR for low-clay samples depend on the pore size, whereas, SVR in clay-rich samples is dominated by clay particles (mainly illite).

adsorption PSD and MI TSD (ρ_2 Visual N2 PSD and ρ_2 Visual MI PSD) as described by Marschall et al. [36] (not shown here). In all calculations the pores are assumed cylindrical and the constant value, c, in Eq. (1) is considered 2.

Although the various PSD measurement techniques should measure the same property in the rock, due to differences in mechanisms and measurement physics, the measured PSD distributions do not probe the same property [40]. To overcome this challenge, we make qualitative comparisons, for example, NMR, MI and N2 distributions for samples with varying clay contents (Figs. 2–6).

Our surface relaxivity calculations allow us to two observations: (a) surface relaxivity varies for different samples and so assumptions of constant surface relaxivity for a formation are not justified; (b) surface relaxivity values depend on the calculation techniques.

In the following sections we investigate the effect of rock composition on surface relaxivity and also explain the sources of discrepancy in surface relaxivity values calculated by different techniques.

5.2. Effect of paramagnetic minerals on surface relaxivity

Fluid–solid interaction (surface relaxation) is usually the dominant relaxation mechanism in porous materials [12] and is quantified by the surface relaxivity both for longitudinal and transverse relaxations. Korringa et al. [30] allocated the longitudinal relaxation of the nuclei at the solid surface to the relaxation of spins at two, magnetic and non-magnetic, surface sites; the spins are temporarily adsorbed to these sites. Kleinberg et al. [28] extended the Korringa et al. [30] model to also account for surface relaxation during transverse relaxation. Using a number of assumptions, the model for longitudinal and transverse relaxations is reduced to [30,28,14]:

$$\frac{1}{T_i} = \left(\frac{Sh}{V}\right)(n_M)\frac{1}{T_{iM}} \tag{3}$$

where i is 1 or 2 to denote longitudinal or transverse relaxation times, respectively, h is the thickness of spin layer that is affected

Table 2
Calculated surface relaxivity using different techniques. ρ_1 and ρ_2N2 SVR: T_1 and T_2 surface relaxivity, respectively using N2 SVR, ρ_2CEC SVR: T_2 surface relaxivity, respectively using CEC SVR, ρ_2 N2 ADS D_{LM}: T_2 surface relaxivity using logarithmic average of pore size form N2 adsorption, ρ_2 MI D_{LM}: T_2 surface relaxivity using logarithmic average of pore size form MI TSD.

Sample #	ρ_1N2 SVR μm/s	ρ_2N2 SVR μm/s	ρ_2CEC SVR μm/s	ρ_2 N2 ADS D_{LM} μm/s	ρ_2 MI D_{LM} μm/s
1	0.70	1.86	0.20	1.99	
2	0.74	1.43	0.30	1.63	
3	0.33	0.50	0.23	0.58	2.08
4	0.26	0.41	0.12	0.53	
5	0.37	0.60	0.23	0.74	1.31
6	0.50	1.06	0.30	1.18	
7	0.58	1.27	0.57	1.38	
8	0.62	1.52	0.29	0.78	
9	0.96	1.70	0.45	0.84	2.72
10	0.71	1.44	0.50	1.72	
11	0.75	1.57	0.33	1.39	
12	0.85	1.39	0.52	1.46	2.36
13	0.76	1.46	0.25	0.74	
14	0.78	1.57	0.36	0.85	
15	1.11	1.71	0.48	0.98	1.73
16	0.61	0.91	0.21	0.58	1.53
17	0.73	1.45	0.16	0.78	
18	0.31	0.39	0.06	0.25	0.87
19	0.61	0.93	0.08	0.74	1.71
20	1.24	2.08	0.72	1.05	1.25
21	0.82	1.29	0.60	1.00	1.53
22	1.19	1.83	1.24	0.92	1.49
23			2.72	4.33	
24	1.04	1.89	0.64	1.05	
25	0.99	2.52	0.70	1.38	
26	1.44	2.54	0.92	1.35	1.53
27	1.07	2.30	1.00	1.29	
28	1.04	1.97	0.94	1.09	

by surface sites, n_M is the ratio of number of magnetic surface sites to the total number of surface sites and T_M is characteristic relaxation of nuclei at magnetic surface sites. Combining Eqs. (1) and (3), the surface relaxivity can be written as:

$$\rho_i = \frac{h n_M}{T_{iM}} \tag{4}$$

The surface relaxivity can be assumed to be a function of the concentration of the magnetic sites if: (a) All the spins relax at the same rate once they contact a magnetic site and (b) the spin layer thickness affected by the surface effect is constant [14]. For simplicity we refer to the non-magnetic sites as the "host mineral" and the magnetic ions, compounds or minerals as "magnetic impurity" or simply "impurity".

Numerous studies have shown the effect of concentration of various magnetic impurities on the surface relaxivity of synthetic porous materials (e.g. [26,14,4,22,23]. We now compare observations from the study of synthetic porous materials with those from our study:

5.2.1. Observation 1: Most of the impurities that are abundant in soil or near-surface depths (oxidizing environments) have very high magnetic susceptibilities

In most cases, the impurities discussed in the literature are ferromagnetic minerals with very high magnetic susceptibility e.g. magnetite, goethite and pyrrhotite. Due to the chemical alteration (digenesis), metamorphism, presence of sulfide-reducing bacteria and changes in oxygen content and acidity (PH) [45], the impurities in hydrocarbon reservoir formations, such as the Bakken Formation, are mainly paramagnetic minerals e.g. pyrite, illite, montmorillonite (smectite) and Fe-chlorite (Chamosite) (Table 3) with orders of magnitudes lower magnetic susceptibility compared to near surface ferromagnetic minerals. Other minerals, formation brine and hydrocarbons are diamagnetic (Table 3) and do not contribute to the enhanced relaxation of the spins at the surface of the minerals.

5.2.2. Observation 2: The magnetic susceptibility of the porous media increases monotonically with the magnetic impurity concentration

Ferromagnetic minerals tend to dominate the magnetic properties of the rock such as magnetic susceptibility, when they constitute more than 0.1 vol% of the rock and the magnetic susceptibility of rock exceeds 5×10^{-3} SI. In their absence, paramagnetic minerals that form more than 1 vol% of the rocks control the magnetic susceptibility of the rock and this value is usually less than 5×10^{-4} SI (any value in between is a combination of paramagnetism and ferromagnetism) [45]. In near surface NMR studies, the rocks mostly contain one type of impurity. However, reservoir rocks contain a mixture of paramagnetic minerals with variable iron contents. To account for variations in paramagnetic mineral

Table 3
The magnetism and magnetic susceptibility of different minerals, fluids and compounds that are abundant in rock samples from oil and gas producing formations. Ferro, Para and Dia stand for ferromagnetic, paramagnetic, and diamagnetic materials. The brine and the hydrocarbon magnetic susceptibilities are for different fluids from various reservoirs. Since the density values are not unique only mass susceptibility is reported. All mineral density values are from webmineral.com [48].

Mineral/compound	Magnetism	Density[d] gr/cm^3	Mass susceptibility SI 10^{-6} m^3/kg	Volume susceptibility SI 10^{-6}
Magnetite[a]	Ferro	5.15	500–1116	2.58E6 to 5.75E6
Goethite[a]	Ferro	3.80	0.35–0.7	1330–2660
Pyrrhotite[a]	Ferro	4.61	50–53	2.31E5 to 2.44E5
Pyrite[b]	Para	5.01	0.3000	1503
Chlorite[c]	Para	3.20	0.0219–0.4843	70–1550
Fe-Chlorite[a] (Chamosite)	Para	3.20	0.9000	2880
Illite[b]	Para	2.75	0.1500	412.50
Montmorillonite[b]	Para	2.35	0.1400	329
Quartz[b]	Dia	2.65	−0.0062	−16.42
Calcite[c]	Dia	2.71	−0.0051	−13.80
Dolomite[c]	Dia	2.84	−0.0134	−38
K-Feldspar[b]	Dia	2.56	−0.0058	−14.85
Kaolinite[a]	Dia	2.6	−0.019	−49.4
Formation Brine[d]	Dia	N/A	−0.7 to −0.4	N/A
Hydrocarbon Fluids[d]	Dia	N/A	−1.04 to −0.96	N/A

[a] Dearing [9].
[b] Dunlop and Özdemir [10].
[c] Tarling and Hrouda [45].
[d] Ivakhnenko [20].

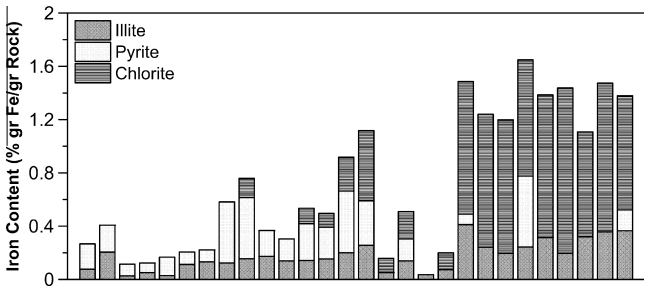

Fig. 8. The iron content for each sample calculated by the iron content in the molecular structure of each mineral. The iron is concentrated mainly in chlorite (chamosite), pyrite and illite with 29.43, 46.55 and 1.43 wt% iron content in their molecular structure, respectively [48].

content, we calculated the iron content of each sample considering the amount of iron in mineral molecular structures (Fig. 8). The iron is concentrated mainly in chlorite (chamosite), pyrite and illite with 29.43, 46.55 and 1.43 wt% iron content in their molecular structure, respectively [48]. Although pyrite has the highest iron content and susceptibility (Fig. 8), illite and chlorite minerals contribute most to the iron content of the rock mainly due to a higher clay content as compared to pyrite content. Fig. 9 shows that pyrite does not affect the susceptibility (Fig. 9a), while a combination of illite and chlorite clay minerals show a direct correlation with susceptibility (Fig. 9b). Near surface NMR studies show a direct correlation between iron bearing mineral content and magnetic susceptibility. However, in sedimentary rocks not all paramagnetic mineral affect the magnetic susceptibility.

5.2.3. Observation 3: The impurities were distributed evenly throughout the porous material by mixing of the grains/powders or chemically coating of the host mineral grain surfaces

Besides their concentration (paramagnetic mineral content), the distribution of the impurities also affects the surface relaxivity. In near surface formations, the impurities are evenly distributed throughout the porous media by chemical coating or mixing of the minerals. In reservoir rocks, the paramagnetic minerals are not distributed uniformly. Pyrite is mainly scattered in the porous media in the form of individual nodules whereas clays can exist as pore-filling material. Scanning electron microscopic (SEM) images revealed that the illite clays (Fig. 10a and b) and to a much lesser extent chlorite clays (Fig. 10c) fill the pore space between the dolomite and quartz grains. Energy dispersive X-ray spectroscopy (EDS) of illite grains (Fig. 10d) confirmed the presence of iron in illite minerals. Distribution of the illite clays in the pore space and their high surface area compared to chlorite and pyrite increases the effect of illite paramagnetic properties on the fluid-rock interaction and consequently surface relaxivity.

5.2.4. Observation 4: Surface relaxivity increases monotonically with increasing impurity concentration

In near surface NMR studies, the surface relaxivity increases linearly with impurity concentration. As discussed earlier, in Bakken samples the only paramagnetic mineral with high concentration (wt%) and that is distributed in the pore space is illite. The plots of ρ_2N2 SVR as a function of different minerals (Fig. 11) confirm that the surface relaxivity has the best correlation with illite (Fig. 11a) compared to chlorite and pyrite which is consistent with the SEM results (Fig. 10). Note that this correlation does not imply that chlorite and pyrite do not affect the surface relaxivity value; it mainly applies to cases where illite clays are distributed in the pore space. More studies are required to investigate the effect of laminated clay content on the surface relaxivity values.

In near surface studies the surface relaxivity and magnetic susceptibility are linearly correlated because commonly one impurity is introduced in the system. However, our result reveals no correlation between susceptibility and surface relaxivity in reservoir rocks (Fig. 11b). We postulate that this is mainly because susceptibility is dominated by chlorite and illite iron content (Fig. 9), whereas the surface relaxivity is dominated by illite content (Fig. 11a).

Other surface relaxivity values (Table 2) have an increasing trend with illite content but with higher scatter and lower correlation coefficients. Similar increasing trends imply that the effect of paramagnetic minerals on surface relaxivity does not depend on calculation method.

5.3. Application of surface relaxivity

The main source of discrepancy in surface relaxivity calculation is correlating NMR data with different SVR, PSD or TSD

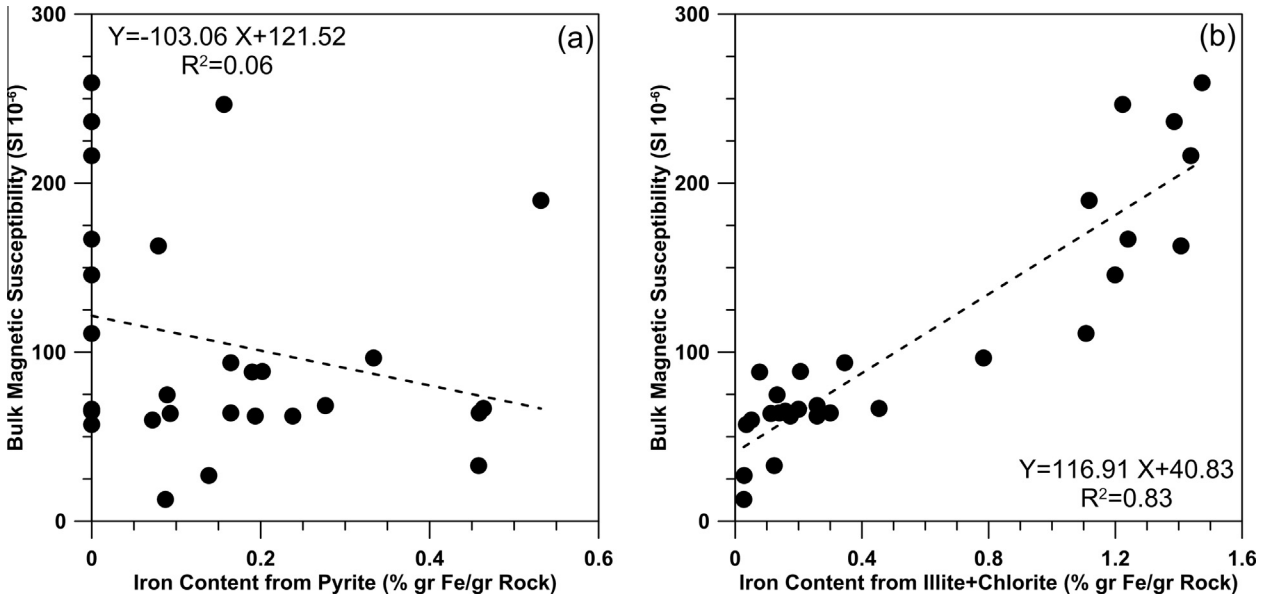

Fig. 9. Cross plot of susceptibility and iron content for (a) pyrite, (b) chlorite and illite minerals. The susceptibility is dominated by the presence of chlorite and illite (mainly chlorite). Due to very low pyrite content (<1 wt%) this mineral does not affect the susceptibility significantly.

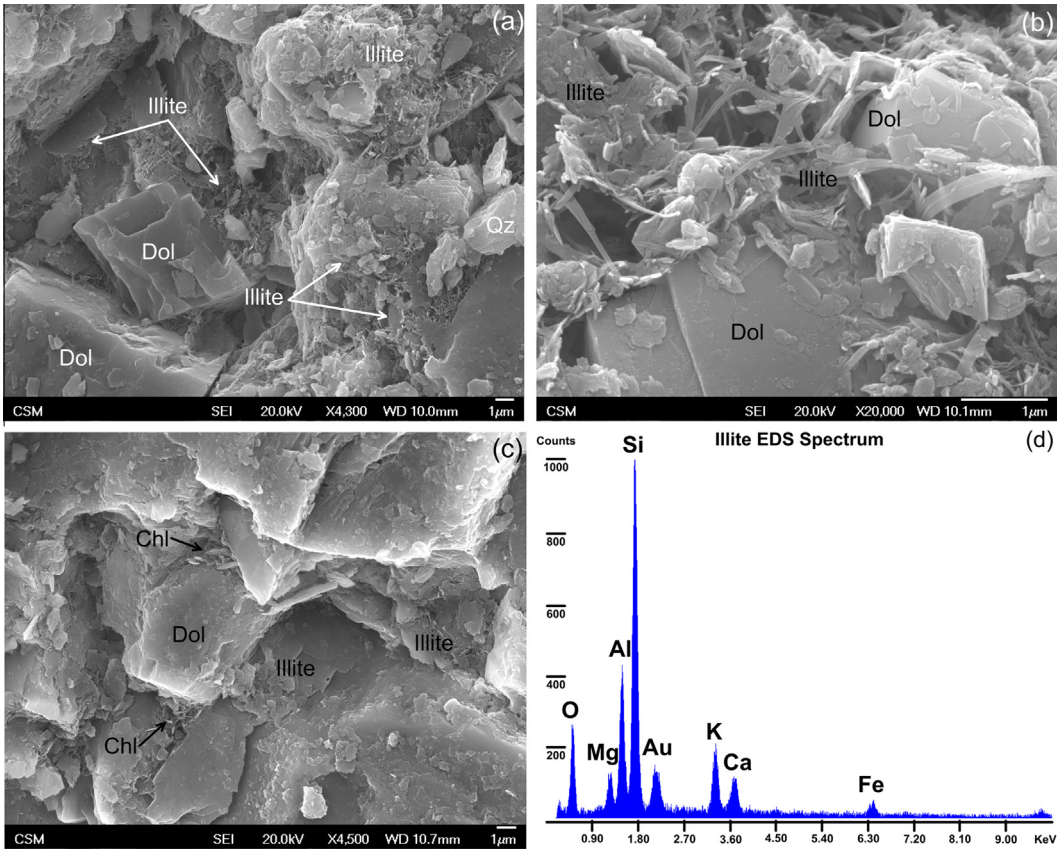

Fig. 10. (a–c) Scanning electron microscopic (SEM) images and (d) energy dispersive X-ray spectroscopy (EDS) for Middle Bakken and Three Forks samples. Illite is distributed in the pore space between large dolomite and quartz grains (a and b). Chlorite is also seen in the space between the dolomite grains, however, due to low chlorite content it is not abundant (c). The EDS data for illite grains show that iron is present in all clays especially illite which has the highest volume.

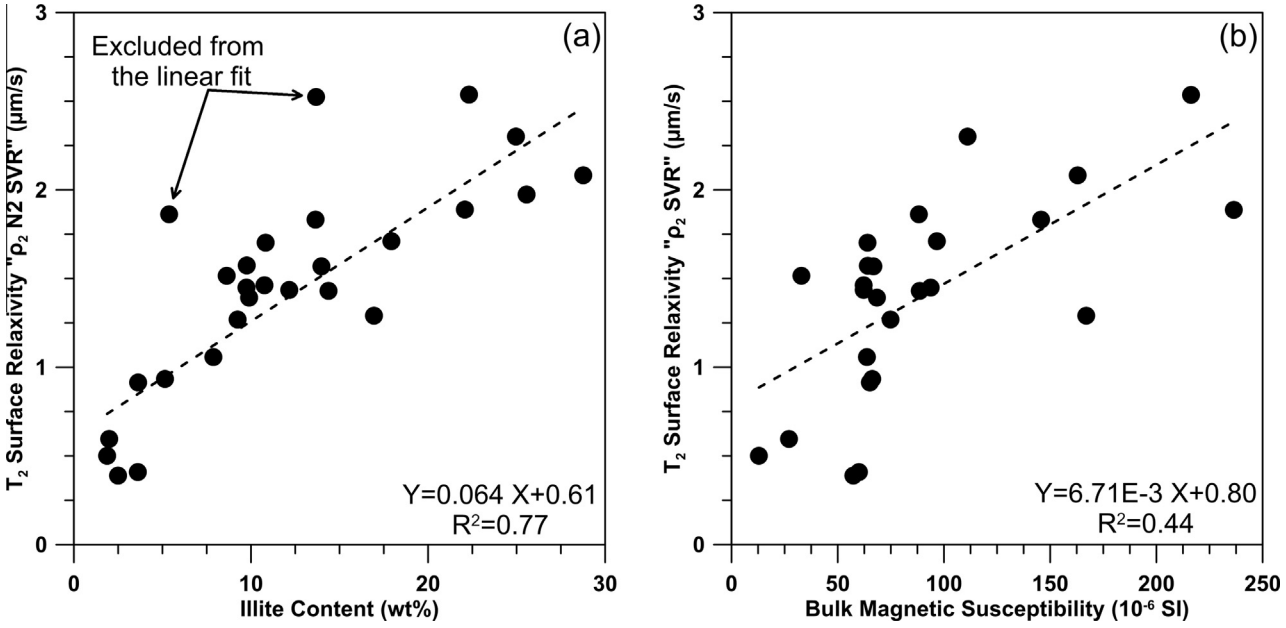

Fig. 11. Correlation between the T_2 surface relaxivity (ρ_2N2 SVR) and (a) illite, (b) susceptibility. The plots of ρ_2N2 SVR as a function of different minerals confirm that the surface relaxivity has the best correlation with illite Note that this correlation does not imply that chlorite and pyrite do not affect the surface relaxivity value. Correlating BMS and surface relaxivity (b) is not a correct approach since BMS value is dominated by chlorite and illite iron (Fig. 9) content whereas the surface relaxivity is dominated by illite content (a).

measurement techniques. These techniques use different mechanisms and physics to assess the same rock property. N2 measurements are based on condensation of N2 in pores with different sizes at different pressures which provide information about the pore body size distribution (Fig. 2). MI measurements are based on the pressure that is required to pass the mercury through pore throats (Fig. 4). In both MI and N2 experiments the investigating fluid has to enter the pore space from the exterior of the sample. As oppose to NMR measurements, in which the sample is fully saturated with the displacement fluid (in most cases water or brine) prior to the measurement and no displacement occurs throughout the experiment.

The other source of discrepancy is assuming similar surface relaxivity for individual pores in the porous media. Theoretically surface relaxivities vary in different pores in the same sample based on the hosting mineral type and the distribution of paramagnetic impurities [2,25]. Measuring this value for individual pores is not practical and a constant surface relaxivity is assumed for PSD or TSD calculation purposes.

We converted the T_2 distributions of two samples both with low and high clay contents to PSD using different calculated surface relaxivities (Figs. 12 and 13, respectively). The following observations can be made: (a) The PSDs calculated from N2 VIS and N2 SVR are similar for both samples. (b) MI VIS and MI DLM also result in similar TSDs. (c) For low clay sample (Fig. 12) the MI TSD data cannot be visually correlated with other techniques whereas the MI TSDs for high clay sample (Fig. 13) are comparable with NMR and N2 data. Note that the value of visually calculated surface relaxivities is biased since there are no specific criteria for a visual good match. This issue is amplified for low clay sample (Fig. 12) samples which show different distribution shapes for all three techniques.

Choosing the appropriate value for practical purposes mainly depends on the application of the PSD or TSD measurements. For example saturation height modeling by correlating MI TSD and NMR data is a common practice in log interpretation and saturation calculation [35,1]. In this case, surface relaxivities calculated by visual correlation between MI TSD and T_2 distribution should be utilized. For permeability calculation using SVR and characteristic pore radius using models such as Kozeny-Carman, the surface relaxivity calculated using Eq. (1) and the measured SVR from N2

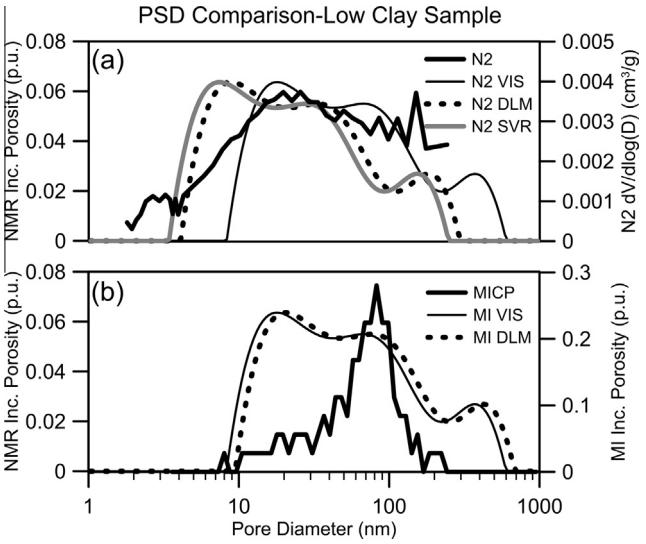

Fig. 12. Different calculated and measured PSD for a low clay sample (a) PSD measured by N2 and NMR converted using the calculated surface relaxivities by combining NMR and N2 measurements. (b) TSD measured by MI and NMR converted using the calculated surface relaxivities by combining NMR and MI measurements.

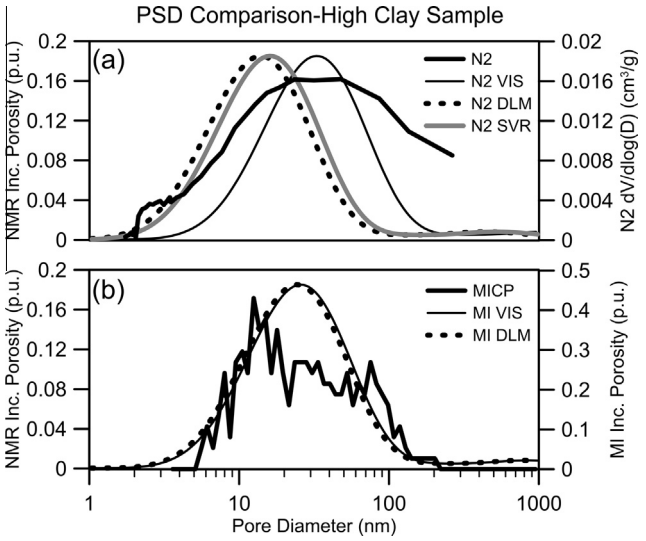

Fig. 13. Different calculated and measured PSD for a clay-rich sample. (a) PSD measured by N2 and NMR converted using the calculated surface relaxivities by combining NMR and N2 measurements. (b) TSD measured by MI and NMR converted using the calculated surface relaxivities by combining NMR and MI measurements.

technique is recommended. We suggest the following steps to utilize the suitable surface relaxivity value for log interpretation purposes:

Step 1: Find the suitable correlation to tie core petrophysical properties to the measured PSD/TSD in the laboratory.
Step 2: Calculate the surface relaxivity using PSD/TSD data.
Step 3: Find a correlation between the calculated surface relaxivity and paramagnetic content of the samples considering the distribution of the minerals and their iron content.
Step 4: Evaluate the mineralogy of the formation and calculate the surface relaxivity using the correlation in step 4.
Step 5: Convert the T_2 or T_1 distributions to PSD or TSD and calculate the petrophysical property of interest using the correlation in step 2.

6. Conclusions

The porosity, pore size distribution and NMR response were measured for 12 Middle Bakken and Three Forks samples. The surface relaxivity was calculated for all samples using different methods. Correlating the surface relaxivity to "distributed" clay content and eventually gamma ray readings at downhole conditions is a novel application of the gamma ray logs in petrophysical characterization of the rocks. Based on the results presented in this study for samples from Middle Bakken and Three Forks formations the following conclusions can be drawn:

- Assuming a constant surface relaxivity for a rock type, formation or well is not accurate and factors such as the content and distribution of paramagnetic mineral should be considered for surface relaxivity calculation.
- We found a linear correlation between surface relaxivity (ρ [μm/s]) and illite content (f_{il} [wt%]) distributed in the matrix $\rho = 0.064 \times f_{il} + 0.61$ with high correlation coefficient ($R^2 = 0.77$).
- Although chlorite and pyrite encompass the highest iron content, illite is uniformly distributed in the pore space and is the paramagnetic impurity that dominates the surface relaxation of hydrogen nuclei at fluid-grain interface.

- Clay bound water cut off times lie between 2.13–2.23 ms for T_1 and 1.34–1.40 ms for T_2 distributions based on our mineralogy-guided calculations. Using typical value of 3 ms resulted in more than 100% error in clay bound porosity calculation especially for high clay content samples.

Acknowledgements

This paper is dedicated to the memory of Dr. Michael L. Batzle. We acknowledge Kurt Livo, Cesar Mapeli and Rana Elghonimy from Colorado School of Mines, Gerhard Heij and Dr. Douglas Elmore from University of Oklahoma, Tomasz Topor from Polish Academi of Science and Douglas McCarty from Chevron ETC for their help in performing some of the measurements. We also acknowledge OCLASSH and Fluids consortiums at Colorado School of Mines for support and funding of the project.

References

[1] Altunbay M, Martain R, Robinson M. Capillary pressure data from NMR logs and its implications on field economics. In: SPE annual technical conference and exhibition, 30 September–3 October. New Orleans, Louisiana, SPE 71703-MS; 2001. doi: http://dx.doi.org/10.2118/71703-MS.
[2] Arns CH, Sheppard AP, Saadatfar M, Knackstedt MA. Prediction of permeability from NMR response: surface relaxivity heterogeneity. In: SPWLA 47th annual logging symposium. Veracruz, Mexico; 2006 June 4–7.
[3] Barrett EP, Joyner LG, Halenda PP. The determination of pore volume and area distributions in porous substances. I. computations from nitrogen isotherms. J Am Chem Soc 1951;73:373–80.
[4] Bryar TR, Daughney CJ, Knight R. Paramagnetic effects of iron(III) species on nuclear magnetic relaxation of fluid protons in porous media. J Magn Reson 2000;142(1):74–85.
[5] Buttler JP, Reeds JA, Dawson SV. Estimating solution of first kind integral equations with non-negative constraints and optimal smoothing. Siam J Numer Anal 1981;18(3):381–97.
[6] Carr H, Purcell E. Nuclear magnetic resonance: petrophysical and logging applications. Phys Rev 1954;94(3):630–8.
[7] Coates GR, Lizhei X, Prammer MG. NMR logging principles and applications. Haliburton Energy Services Publication; 1999.
[8] Comisky J, Santiago M, McCollom B, Buddahala A, Newsham K. Sample size effects on the application of mercury injection capillary pressure for determining the storage capacity of tight gas and oil shales: Canadian Unconventional Resources Conference. SPE Paper 149432; 2011, doi: http://dx.doi.org/10.2118/149432-MS.
[9] Dearing J. Environmental magnetic susceptibility using the Bartington MS2 system. Bartington Instruments Limited; 1999.
[10] Dunlop DJ, Özdemir Ö. Rock magnetism: fundamentals and frontiers. Cambridge University Press; 1997.
[11] Dunn KJ, LaTorraca GA, Warner JL, Bergman DJ. On the calculation of NMR relaxation time distributions. In: SPE 69th annual technical conference and exhibition, New Orleans, 25–28 September. SPE 28367; 1994.
[12] Dunn KJ, Bergman DJ, LaTorraca GA. Nuclear magnetic resonance: petrophysical and logging applications. Pergamon: Elsevier Science; 2002.
[13] Fleury M. NMR surface relaxivity determination using NMR apparent diffusion curves and BET measurements. In: Society of core analysis, Calgary, Canada, 10–12 September, SCA2007-35; 2007.
[14] Foley I, Farooqui SA, Kleinberg RL. Effect of paramagnetic Ions on NMR relaxation of fluids at solid surfaces. J Magn Reson, Ser A 1996;123(1):95–104.
[15] Gregg SJ, Sing KSW. Adsorption, surface area, and porosity. 2nd ed. New York: Academic Press; 1983.
[16] Harkins DW, Jura G. Surfaces of solids. XII. An absolute method for the determination of the area of a finely divided crystalline solid. J Am Chem Soc 1944;66(8):1362–6. http://dx.doi.org/10.1021/ja01236a048.
[17] Hossain Z, Grattoni CA, Solymar M, Fabricius IL. Petrophysical properties of greensand as predicted from NMR measurements. J Petrol Geosci 2011;17:111–25. http://dx.doi.org/10.1144/1354-079309-038.
[18] Howard JJ, Kenyon WE, Straley C. Proton magnetic resonance and pore size variations in reservoir sandstones. SPE Formation Eval 1993;8(3):194–200. http://dx.doi.org/10.2118/20600-PA.
[19] Hürlimann MD, Helmer KG, Latour LL, Sotak CH. Restricted diffusion in sedimentary rocks. Determination Surf Area Volume Ratio Surf Relaxivity 1994;111(2):169–78. http://dx.doi.org/10.1006/jmra.1994.1243.
[20] Ivakhnenko OP. Magnetic susceptibility of petroleum reservoir crude oils in petroleum engineering. In: Younes MAA, editor. Crude oil exploration in the world. Intech; 2012. p. 71–8.
[21] Jiang T, Rylander E, Singer PM, Lewis RE, Sinclair SM. Integrated petrophysical interpretation of eagle ford shale with 1-D and 2-D nuclear magnetic resonance. In: SPWLA 54th annual logging symposium; 2013, 22–26 June.
[22] Keating K, Knight R. A laboratory study to determine the effect of iron oxides on proton NMR measurements. Geophysics 2007;72(1):E27–32.
[23] Keating K, Knight R. A laboratory study of the effect of magnetite on NMR relaxation rates. J Appl Geophys 2008;66(3–4):188–96.
[24] Keating K, Knight R. A laboratory study of the effect of Fe(II)-bearing minerals on nuclear magnetic resonance (NMR) relaxation measurements. Geophysics 2010;75(3):F71–82.
[25] Keating K, Knight R. The effect of spatial variation in surface relaxivity on nuclear magnetic resonance relaxation rates. Geophysics 2012;77(5):E365–77.
[26] Kenyon WE, Kolleeny JA. NMR surface relaxivity of calcite with adsorbed Mn^{2+}. J Colloid Interface Sci 1995;170(2):502–14.
[27] Kenyon WE. Petrophysical principles of applications of NMR logging. Log Anal 1997;38(2):21–43.
[28] Kleinberg RL, Kenyon WE, Mitra PP. Mechanism of NMR relaxation of fluids in rock. J Mag Reson-Ser A 1994;108(2):206–14. http://dx.doi.org/10.1006/jmra.1994.1112.
[29] Kleinberg RL. Utility of NMR T_2 distributions, connection with capillary pressure, clay effect, and determination of the surface relaxivity parameter, ρ_2. Mag Reson Imaging 1996;14(7–8):761–7. http://dx.doi.org/10.1016/S0730-725X(96)00161-0.
[30] Korringa J, Seevers DO, Torrey HC. Theory of spin pumping and relaxation in systems with a low concentration of electron spin resonance centers. Phys Rev 1962;127(4):1143–50. http://dx.doi.org/10.1103/PhysRev. 127.1143.
[31] Kuila U. Measurement and Interpretation of Porosity and Pore-Size Distribution in Mudrocks: the Hole Story of Shales. Ph.D. Thesis. Colorado School of Mines; 2013.
[32] Kuila U, McCarty DK, Derkowski A, Fischer TB, Prasad M. Total porosity measurement in gas shales by the water immersion porosimetry (WIP) method. J Fuel 2014;117(Part B):1115–29. http://dx.doi.org/10.1016/j.fuel.2013.09.07.
[33] Latour LL, Mitra PP, Kleinberg RL, Sotak CH. Time-dependent diffusion coefficient of fluids in porous media as a probe of surface to volume ratio. J Magn Reson, Ser A 1993;101(3):342–6.
[34] Lawson CL, Hanson RJ. Solving least square problems. Englewood Cliffs, New Jersey: Prentice-Hall; 1974.
[35] Lowden BD, Porter MJ, Powrie LS. T_2 relaxation time versus mercury injection capillary pressure: implications for NMR logging and reservoir characterization. In: SPE European petroleum conference, 20–22 October, Hague, Netherlands, SPE 50607; 1998, doi: http://dx.doi.org/10.2118/50607-MS.
[36] Marschall D, Gardner JS, Mardon D, Coates GR. Method for correlating NMR relaxometry and mercury injection data. In: Society of core analysis conference, SCA 9511; 1995.
[37] Meiboom S, Gill D. Modified Spin-Echo method for measuring nuclear relaxation times. Rev Sci Instr 1958;29(8):668–91.
[38] Mitra PP, Sen PN, Lawrence MS, Doussal PL. Diffusion propagator as a probe of the structure of porous media. Phys Rev Lett 1992;68(24):3555–8.
[39] Rivera S, Saidian M, Godinez LJ, Prasad M. Effect of mineralogy on NMR, sonic, and resistivity: a case study of the Monterey Formation. In: Unconventional resources technology conference, August 25–27. Denver, CO, URTeC 1922872; 2014, doi: http://dx.doi.org/10.15530/urtec-2014-1922872.
[40] Saidian M, Kuila U, Prasad M, Alcantar-Lopez L, Rivera S, Godinez LJ. A comparison of measurement techniques for porosity and pore size distribution in mudrocks: a case study of Haynesville, Niobrara, Monterey and Eastern European Silurian Formations. In: AAPG Memoir 110: Imaging unconventional reservoir pore systems. AAPG Bull [in press].
[41] Saidian M. Effect of rock composition and texture on pore size distributions in shales: applications in low field nuclear magnetic resonance. Ph.D. Thesis, Colorado School of Mines; 2015.
[42] Sen PN, Straley C, Kenyon WE, Whittingham MS. Surface-to-volume ratio, charge density, nuclear magnetic relaxation, and permeability in clay-bearing sandstones. Geophysics 1990;55(1):61–9. http://dx.doi.org/10.1190/1.1442772.
[43] Slijkerman WFJ, Hofman JP. Determination of surface relaxivity from NMR diffusion measurements. Magn Reson Imaging 1998;16(5–6):541–4.
[44] Straley C, Roosini D, Vinegar H, Tutunjian P, Morriss C. Core analysis by low field NMR. Log Anal 1997;38(2):84–94.
[45] Tarling DH, Hrouda F. The magnetic anisotropy of rocks. Chapman and Hall; 1993.
[46] Timur A. Pulsed nuclear magnetic resonance studies of porosity, movable fluid and permeability of sandstones. J Petrol Technol 1969;21(6):775–86.
[47] Washburn EW. The dynamics of capillary flow. Phys Rev Lett 1921;17(3):273–83. http://dx.doi.org/10.1103/PhysRev. 17.273.
[48] Webmineral Website Database. Webmineral.com\data\; 2015.
[49] Yao Y, Liu D. Comparison of low-field NMR and mercury intrusion porosimetry in characterizing pore size distributions of coals. Fuel 2012;95(5):152–8.